USING DENSITY INVARIANT GRAPH LAPLACIAN TO RESOLVE UNOBSERVABLE PARAMETERS FOR THREE-DIMENSIONAL OPTICAL BIO-IMAGING

Chien-Hung Lu and Pei-Yuan Wu

Department of Electrical Engineering, Princeton University, NJ, 08540
appl.chlu@gmail.com, peiwu@princeton.edu

ABSTRACT

We explore the graph Laplacian eigenmap for the application of three-dimensional (3D) optical bioimaging. By using the density invariant graph Laplacian, each high-dimensional sampling (e.g. an image) could be represented by a low-dimensional description. These descriptions not only preserve key features of raw images but also estimate unobservable parameters for 3D imaging. In this paper, we apply this method for two 3D optical microscopies under following scenarios: (i) 3D optical tomography with projections of unknown orientation. (ii) 3D deconvolution microscopy with a disordered focal stack. To prove the robustness of the method, we use images from real biological systems and experimental measurements. In both cases, our results show that the density invariant graph Laplacian is able to overcome practical issues such as limited number of measurement, unstable environment, misalignment and experimental noise.

Index Terms— optical tomography, 3D bio-imaging, dimension reduction, manifold learning

1. INTRODUCTION

Dimension reduction is employed by a variety of fields such as machine learning, data mining, computer graphics and vision. The main idea is to give a simple representation of high-dimensional data which preserves meaningful features and further estimates unobservable parameters in raw data set. One popular technique of dimension reduction is the graph Laplacian method. This graph-based algorithm has advantages of its simplicity, interpretability and provides efficient representation for complex data structure [1–3]. It has been used for bio-signal and bio-image processing such as spike sorting of neural signal [4], protein function prediction [5], image classification of MRI [6] and retinal layered image segmentation [7]. The application on 3D reconstruction of bioimaging is first addressed by Ronald R. Coifman *et al* [8,9] for cryo-electron microscopy (Cryo-EM), in which hundreds to thousands unknown orientations of view of a molecule could be ordered so that reconstructing 3D structure of a single molecule is possible. However, care must be taken in this method for further applications. Generally, physical images measured in laboratory don't lie on a simple manifold because lots of uncontrollable factors such as stray light, shot noise, thermal fluctuation, mechanical vibration, misalignment, and random motion of sample would result in a complicated high-dimensional manifold. The graph Laplacian therefore cannot provide simple descriptions that preserve the desired features of raw image set. For example in Cryo-EM microscopy, the dynamics of molecule is uncontrollable so that the orientation of measured images randomly distribute on the unit spherical surface of the Euclidean space. Moreover, because of weak electron scattering of single molecule, Cryo-EM image has very low signal-to-noise ratio. As a result, these samplings lie on a very complicate high-dimensional manifold (e.g. a rough surface) and simple graph-based method cannot give accurate estimate of unobservable parameters [8–11]. Second, almost all applications in bioimaging have limited number of measurements due to dose-limit, photo-damage, short life time, and quick morphological change of biological system. In most cases, one cannot get enough sampling number to meet theoretical assumptions (e.g. $N \to \infty$).

Motivated by these concerns, here we examine the graph Lapalcian method by considering these practical issues in bioimaging. Our contributions of this paper are (i) using the density invariant graph Laplacian operator to handle non-uniform samplings in high-dimensional space. (ii) extending the method to 3D optical microscopy for bio-features in micrometer scale under limited number of measurement.

1.1. Relation to prior work

The work presented here is focused on 3D optical microscopy based on multiple 2D images, which takes advantage of the density invariant graph Laplacian operator. The work by Raheleh Kafieh *et al* [7] and Hang Su *et al* [12] consider only segmentation of a single 2D microscopic image, and the work by Yasser Ghanbari *et al* [4] considers only time-domain analysis, and the work by A. Singer and H.-T. Wu [11] considers only 2D tomography for large number of sampling on a phantom model. The work by Russell Fung *et al* [13] takes a different approach in spatial frequency domain based on generative topographic mapping. The presented study capitalizes both new imaging scales and new biological systems, which were not considered in these earlier studies.

978-1-4799-2893-4/14/$31.00 ©2014 IEEE

2. DENSITY INVARIANT GRAPH LAPLACIANS FOR 1D MANIFOLD EMBEDDING

We first review the density invariant graph Laplacian method. Consider a one-dimensional smooth manifold Γ with total length $2\pi\alpha$, and let $g : \mathbb{R} \to \Gamma$ be an arc-length preserving onto mapping with period 2π such that $\text{arc}(g(\theta_x), g(\theta_y)) = \alpha(\theta_y - \theta_x)$[1] whenever $|\theta_y - \theta_x| < 2\pi$. Next, denote $k(x, y) = k(\|x - y\|) = \exp\left(-\frac{\|x-y\|^2}{2\varepsilon}\right)$ be a Gaussian kernel. For a smooth function $f : \Gamma \to \mathbb{R}$ and fixed point $x \in \Gamma$, consider $\tilde{f}(\theta) = f(g(\theta))$ and take $\theta_x \in g^{-1}(x)$. Depending on the curvature of Γ near x, the following approximation holds valid if θ_y is sufficiently close to θ_x:

$$\begin{aligned} k(g(\theta_x), g(\theta_y)) &\approx k(|\text{arc}(g(\theta_x), g(\theta_y))|) \\ &= \exp\left(-\frac{\alpha^2(\theta_x - \theta_y)^2}{2\varepsilon}\right) \stackrel{\text{def}}{=} k_\theta(\theta_x, \theta_y) \end{aligned} \tag{1}$$

Given N samples $\{x_i\}_{i=1}^N$, our goal is to find θ_i such that $g(\theta_i) = x_i$ for each sample x_i. Let $q(\theta)$ be the sampling probability density function on Γ. As $N \to \infty$, one has [14]

$$\frac{\sum_{i=1}^N k(x, x_i) f(x_i)}{\sum_{i=1}^N k(x, x_i)} = \int_{\theta_x - \pi}^{\theta_x + \pi} \rho(\theta_x, \theta)\tilde{f}(\theta)d\theta + O(\frac{\varepsilon^{1/4}}{N^{1/2}}) \tag{2}$$

where

$$\begin{aligned} \rho(\theta_x, \theta) &= \frac{k_\theta(\theta_x, \theta)q(\theta)}{\int_{\theta_x - \pi}^{\theta_x + \pi} k_\theta(\theta_x, \theta)q(\theta)d\theta} \\ &\simeq \frac{\alpha}{\sqrt{2\pi\varepsilon}}\exp\left(-\frac{\alpha^2(\theta_x - \theta)^2}{2\varepsilon}\right) \end{aligned} \tag{3}$$

assuming uniform sampling case $q(\theta) = \frac{1}{2\pi}$.

Next, consider the Taylor expansion of $\tilde{f}(\theta)$ near θ_i:

$$\begin{aligned} &\int_{\theta_x - \pi}^{\theta_x + \pi} \rho(\theta_x, \theta)\tilde{f}(\theta)d\theta \\ &= \int_{\theta_x - \pi}^{\theta_x + \pi} \rho(\theta_x, \theta)\left(\sum_{m=0}^{3} \frac{(\theta - \theta_x)^m}{m!}\frac{d^m}{d\theta^m}\tilde{f}(\theta_x) + O((\theta - \theta_x)^4)\right)d\theta \\ &= \tilde{f}(\theta_x) + \frac{\varepsilon}{2\alpha^2}\tilde{f}''(\theta_x) + O(\varepsilon^2) \end{aligned} \tag{4}$$

Note that the elimination of the 1st and 3rd-order terms in (4) relies on the symmetry of $\rho(\theta_x, \theta)$. For non-uniform sampling case, since $q(\theta)$ is not constant, the 1st and 3rd-order terms in (4) might not be dropped. To solve the problem, the Gaussian kernel is redefined by $\tilde{k}(x, y) = \frac{k(x,y)}{q(x)q(y)}$ to normalize the effect of the density function. Then combing (2) and (4), the Gaussian kernel $\tilde{k}(x, y)$ is estimated by Laplacian operator:

$$\frac{\sum_{i=1}^N \tilde{k}(x, x_i) f(x_i)}{\sum_{i=1}^N \tilde{k}(x, x_i)} - f(x) \approx \frac{\varepsilon}{2\alpha^2}\tilde{f}''(\theta_x) + O(\varepsilon^2) \tag{5}$$

Next, we consider the finite number of sampling N by constructing a kernel matrix $K \in \mathbb{R}^{N\times N}$ s.t. $K_{ij} = k(x_i, x_j)$, and a diagonal matrix $D \in \mathbb{R}^{N\times N}$, $D_{ii} = \sum_{j=1}^N K_{ij}$. Here, we estimate $q(x_i) \propto D_{ii}$ as in [2]. Then the normalized kernel matrix $\tilde{K} = D^{-1}KD^{-1}$, $\tilde{K}_{ij} = \tilde{k}(x_i, x_j)$. Finally we get the density invariant graph Laplacian operator $L \equiv \tilde{D}^{-1}\tilde{K} - I$, $\tilde{D}$ is another diagonal matrix, $\tilde{D}_{ii} = \sum_{j=1}^N \tilde{K}_{ij}$, and I is the identity matrix. For any vector $\mathbf{f} = [f(x_1), \cdots, f(x_N)]^T$, the i-th component of $L\mathbf{f}$ satisfies:

$$\begin{aligned} (L\mathbf{f})_i &= \frac{(\tilde{K}\mathbf{f})_i}{\tilde{D}_{ii}} - (\mathbf{f})_i = \frac{\sum_{j=1}^N \tilde{k}(x_i, x_j)f(x_j)}{\sum_{j=1}^N \tilde{k}(x_{p_i}, x_{p_j})} - f(x_i) \\ &\approx \frac{\varepsilon}{2\alpha^2}\tilde{f}''(\theta_i) + O(N^{-1/2}\varepsilon^{-1/4}, \varepsilon^2) \end{aligned} \tag{6}$$

Namely, L approximates the Laplacian operator. Note that for finite number of sampling, there is additional error term related to $N^{-1/2}\varepsilon^{-5/4}$ addressed by [15].

Eq (6) implies that considering any eigenvector $\boldsymbol{\psi}$ of L is roughly equal to considering $\tilde{f}''(\theta) = -\lambda\tilde{f}(\theta)$. Impose boundary condition $\tilde{f}(0) = \tilde{f}(2\pi)$, the first two harmonic eigenfunctions are $cos(\theta)$ and $sin(\theta)$. Therefore, excluding the trivial eigenvector (i.e. $\psi_0 = [1, 1, ..., 1]^T$, L has the first two non-trivial eigenvetors $\boldsymbol{\psi}_1, \boldsymbol{\psi}_2$ whose i-th component $(\boldsymbol{\psi}_1)_i \propto cos(\theta_i)$ and $(\boldsymbol{\psi}_2)_i \propto sin(\theta_i)$. Finally, the wanted parameters θ_i are obtained by:

$$\theta_i = \begin{cases} \tan^{-1}\frac{(\boldsymbol{\psi}_2)_i}{(\boldsymbol{\psi}_1)_i} & \text{, if } (\boldsymbol{\psi}_1)_i \geq 0 \\ \tan^{-1}\frac{(\boldsymbol{\psi}_2)_i}{(\boldsymbol{\psi}_1)_i} + \pi & \text{, if } (\boldsymbol{\psi}_1)_i < 0 \end{cases} \tag{7}$$

Considering the error balance between ε and N, the optimal choice of $\varepsilon = \frac{C(\Gamma)}{N^{2/7}}$ that minimizes the error term is suggested by [14], where $C(\Gamma)$ is a constant which depends on the length and curvature of Γ.

3. THE DENSITY INVARIANT GRAPH LAPLACIAN FOR 3D BIOIMAGING

In the previous section, we assume that all samples lie on a one-dimensional manifold. Is this true for real experimental data? The general answer is negative even under the assumption of perfect measurement. For example, considering a set of images of a rational object taken from different Euler angles (θ, ϕ). These images must lie on a two-dimensional manifold because the rotational motion requires two parameters to be fully described. Using one parameter inevitably losses information. However, the assumption of one-dimensional manifold might be valid if we could limit one degree of freedom of the object motion (e.g., rotate along a fixed axis). Recently, because of the rapid development of optically-induced micromanipulation, the manipulation of bio-object to translate or rotate under certain degree of freedom is possible. One popular technique is optical tweezer [16, 17], which is able to trap and rotate a bio-object along a fixed rotation axis. Another example is using opto-microfluidics to give desired

[1] $\text{arc}(x, y)$ denotes the directional arc length from x to y on Γ.

speed and motion of flowing sample in microfluidic channel [18, 19]. However, in both methods, there are limitations against precise control. In the former method, the focusing laser beam leads to nonlinear response of material, which makes linear control a difficult task. In the latter method, the complexity of fluid system and non-rigid motion of flowing object usually result in unpredictable movement. Despite the spatial and angular uncertainty of these methods, these experimental techniques are able to limit the motion of an object along a fixed degree of freedom. The density invariant graph Laplcian therefore could overcome these uncertainties mentioned above. To verify this idea, we examine the density invariant graph Laplacian in the following two subsections.

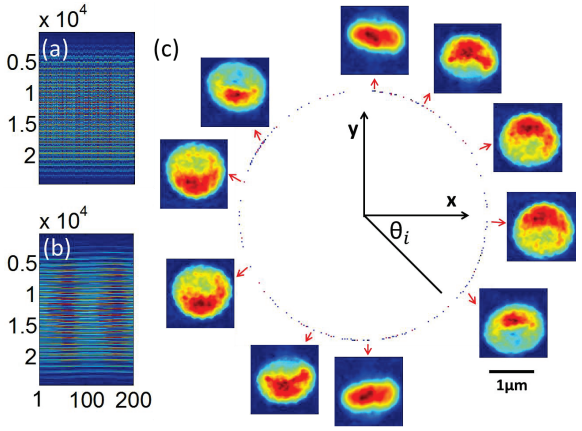

Fig. 1. (a) before and (b) after applying the density invariant graph Laplacian algorithm, the horizontal axis shows the number of vector. (c) projections at different orientations embedded in a unit circle of the Euclidean plan. Clockwise, it shows the rotation of the yeast cell along a fixed axis.

3.1. Optical tomography of a yeast cell

Optical tomography reconstructs 3D volume image of a bio-object by measuring multiple projections at different observation angles ϕ. Instead of moving the light source, optical tomography rotates sample due to the stability requirement on optical setup. The undetermined rotational position therefore would destroy tomographic reconstruction. Here we consider the worst case: the angle of rotation ϕ is totally missing. We use a volume image of a yeast cell which was reconstructed by an X-ray diffraction tomographic algorithm [20] using known projections measured at Spring-8 synchrotron radiation institute [21]. From the reconstructed yeast cell, we randomly generate N projections with rotation angle uniformly distributed in $[0, 2\pi]$, and convert each projection to a row vector, denoted by $x_1, x_2, ..., x_N$. Then we normalize each vector by dividing the L_2-norm of the mean vector $\bar{x} = \frac{\sum_i x_i}{N}$. In this example, we set $\varepsilon = \frac{C(\Gamma)}{N^{2/7}} = 0.8$. Fig. 1(a) shows N=200 vectors, and we can see that the order is indeed shuffled due to the random projection angels. After applying the density invariant graph Laplacian algorithm, we obtain $\{\theta_i\}_{i=1}^N$. Then we are able to reorder these vectors by sorting $\{\theta_i\}$, as shown in Fig. 1(b). In Fig. 1(c), we can see the rotation of the yeast cell, where each projection corresponds to a point embedded in a unit circle. Denote the sorted vector set by $\{x_{\phi_i}\}_{i=1}^N$, we then estimate $\{\phi_i = \frac{2\pi i}{N}\}_{i=1}^N$ based on uniformly distribution. Fig. 2 shows the variance between estimated and actual angle ϕ_i. We found that in the case of N=200, the estimate is accurate to actual angle, it gives a RMS error of 5.35^o, and N=100 gives the RMS error of 10.64^o. The variance of N=50 gives the largest RMS error of 13.14^o and has a reversed ordering of estimate, which would lead to a mirrored reconstruction.

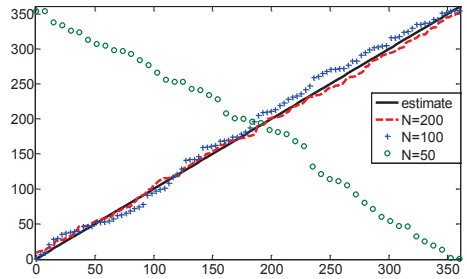

Fig. 2. the error between estimated and actual angle ϕ_i. Black solid line shows the estimate $\phi_i = \frac{2\pi i}{N}$; red dash line, blue cross and green circle show actual angle ϕ_i using number of projection N = 200, 100, and 50, respectively.

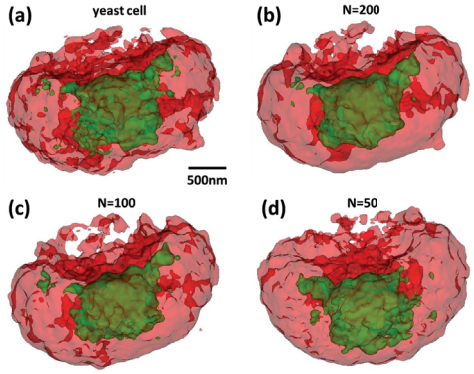

Fig. 3. (a) the yeast cell. (b-d) reconstruction using the number of random projection N=200, 100, and 50, respectively.

By using these estimates, we perform a tomography algorithm, filter-back-projection (FBP), to reconstruct 3D volume image. Fig. 3(a) shows the original yeast cell, and Fig 3(b-d) shows the tomographic reconstruction using N=200, 100, and 50 projections, respectively. We found that these reconstructions preserve big features such as the nuclear and membrane, although losing some high-frequency components when compared to the original yeast cell. In the N=50 case, we also found that the mirrored object is reconstructed due to the reversed estimate of angle. Since we have accurate estimates, it suggests that using better tomographic algorithm such as Fourier-slice method [22] would get more details of the original yeast cell.

3.2. Ordering a focal stack of a zebrafish embryo for 3D deconvolution microscopy

Deconvolution microscopy reconstructs 3D image by measuring the focal stack of an object. In this method, the sample has to be fixed and a translator scans across focal plans. If the measurement is in a dynamic environment (e.g. in flowing fluid) or the sample has random motions, it results in an imprecise focal stack. Here, to give a proof-of-principle experiment, we take a focal stack of a 24 hfp zebrafish embryo as the ground truth and then shuffle the focal stack to generate a totally disordered focal stack (see video1[2]). We then convert each image to a row vector, denoted by $x_{z_1}, x_{z_2}, ..., x_{z_N}$. Here $\{z_i\} \subset \mathbb{R}$ denotes random variable of depth position. Then we normalize each vector by dividing the L_2-norm of the mean vector $\bar{x} = \frac{\sum_i x_{z_i}}{N}$. Fig. 4(a) shows N=61 vectors, and we can see that the ordering is totally shuffled due to the random z-position. After applying the density invariant graph Laplacian method (see Eq. (6) and (7)), we obtain $\{\theta_i\}_{i=1}^N$ and are able to get the sorted focal stack according to $\{\theta_i\}$, as shown in Fig. 4(b). In Fig. 4(c), we can see each image as an embedded point in a unit circle, and these images show focusing and defocusing effects with different depths (see video2[3]). Clockwise, we can observe that the refocusing from the right eye to the left eye of the zebrafish embryo. We also found a big jump near twelve o′clock due to finite z-position (i.e. $\{z_i\} \subset [-d, d], d < \infty$).

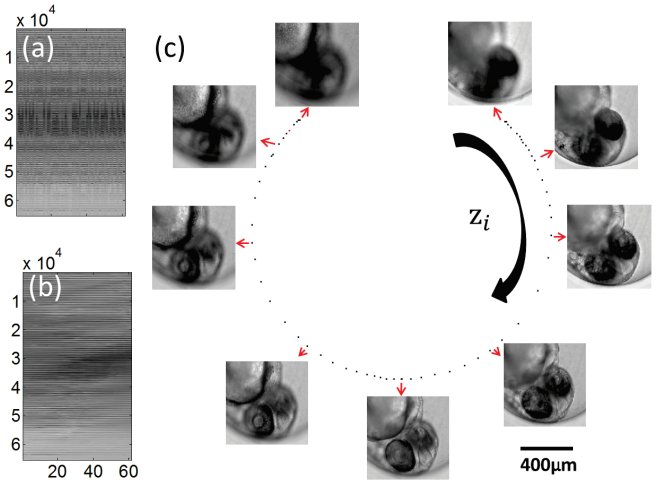

Fig. 4. (a) before and (b) after applying the density invariant graph Laplacian algorithm. (c) images at different depths embedded in a unit circle. Clockwise, the refocusing from the right eye to the left eye of the 24 hfp zebrafish embryo.

Note that in this experiment, we set $\varepsilon = \frac{C(\Gamma)}{N^{2/7}} = 0.0062$, but it is not necessary to use this particular value. Fig. 5 shows the relation between different ϵ values and the estimating error. Fig. 5(a) shows that there is no swap if $\varepsilon \in [0.001, 0.0074)$, and there is one pair of fame (#56 and #57) swapped if $\varepsilon \in [0.0074, 0.025)$, and there is one more swapped pair of frame (#51 and #52) if $\varepsilon \in [0.025, 0.1]$. Fig. 5(b-d) shows the estimated and actual frame number corresponding to these three different ranges of ε.

[2]https://sites.google.com/site/chienhungluke/research/video1.mp4
[3]https://sites.google.com/site/chienhungluke/research/video2.mp4

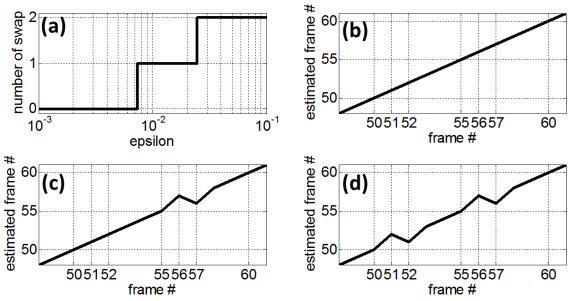

Fig. 5. (a) error versus different ε values. (b-d) actual versus estimated frame number using $\varepsilon \in [0.001, 0.0074)$, $[0.0074, 0.025)$, and $[0.025, 0.1]$, respectively.

The correct reordering for disordered focal stack implies that the density invariant Laplacian operator accounts for wave optics: it is able to find the law of wave propagation without physical prior knowledge. Also, the zebrafish embryo contains lots of bio-features such as eyes, digestive system and heart, especially, in the upper part of the frame #15 to #30 of video 2, we can even observe the heart beating of the zebrafish embryo in the correct time sequence. If including physical or biological prior knowledge, the density invariant Laplacian method might be able to track non-rigid motion such as respiratory gating [23] in micro-scaled living system. Finally, 3D image could be reconstructed by using the sorted focal stack. It requires the calibration of point-spread-function and the characterization of the optical system in order to design a proper deconvolution algorithm [24]. These details need more paragraphs and it is beyond the scope of this paper.

4. CONCLUSION

In this paper, we apply the density invariant Laplacian method to resolve unobservable parameters for 3D optical microscopy. In the case of losing angular or depth information, our results give accurate estimates of unobservable parameters in experimental images and video. We believe that the presented analysis is not only for the extension of the graph Laplacian method, but also for general interest of bioimaging techniques such as light microscopy, optical tomography, endoscopy, and fluorescence microscopy.

The authors thank Jianwei Miao and Huaidong Jiang for the X-ray diffraction data, and thank Jason Fleischer, Granton Jindal and Jessica Williams for the information and the preparation of the zebrafish embryo.

5. REFERENCES

[1] M. Belkin and P. Niyogi, "Laplacian eigenmaps for dimensionality reduction and data representation," *Neural Comput.*, vol. 15, pp. 1373–1396, 2003.

[2] R. R. Coifman and S. Lafon, "Diffusion maps," *Appl. Comput. Harmon. Anal.*, vol. 21, pp. 5–30, 2006.

[3] Y. Kim and M. Mesbahi, "On maximizing the second smallest eigenvalue of a state-dependent graph laplacian," *IEEE Trans. Automatic Control*, vol. 51, no. 1, 2006.

[4] Y. Ghanbari, P. Papamichalis, and L. Spence, "Graph-laplacian features for neural waveform classification," *IEEE Transactions on Biomedical Engineering*, vol. 58, no. 5, 2011.

[5] L. Tran, "Application of three graph laplacian based semi supervised learning methods to protein function prediction problem," *International Journal on Bioinformatics & Biosciences*, vol. 3, no. 2, p. 11, 2013.

[6] H.-H. Chang, J. M. F. Moura, Y. L. Wu, and C. Ho, "Automatic detection of regional heart rejection in uspio-enhanced mri," *IEEE Transactions on Biomedical Engineering*, vol. 27, no. 8, 2008.

[7] R. Kafieh, M. A. Hossein Rabbani, and M. Sonka, "Intra-retinal layer segmentation of optical coherence tomography using diffusion map," *IEEE International Conference on Acoustics, Speech and Signal Processing (ICASSP)*, 2013.

[8] R. R. Coifman, Y. Shkolnisky, F. J. Sigworth, and A. Singer, "Graph laplacian tomography from unknown random projections," *IEEE Trans. Image Processing*, vol. 17, no. 10, 2008.

[9] R. R. Coifman, Y. Shkolnisky, F. J. Sigworth, and A. Singer, "Reference free structure determination through eigenvectors of center of mass operators," *Appl. Comput. Harmon. Anal.*, vol. 28, pp. 296–312, 2010.

[10] A. Singer and Y. Shkolnisky, "Three-dimensional structure determination from common lines in cryo-em by eigenvectors and semidefinite programming," *SIAM Journal on Imaging Sciences*, vol. 4, no. 2, pp. 543–572, 2011.

[11] A. Singer and H.-T. Wu, "Two-dimensional tomography from noisy projections taken at unknown random directions," *SIAM Journal on Imaging Sciences*, vol. 6, no. 1, pp. 136–175, 2013.

[12] H. Su, Z. Yin, S. Huh, and T. Kanade, "Cell segmentation in phase contrast microscopy images via semi-supervised classification over optics-related features," *Medical Image Analysis*, vol. 17, pp. 746–765, 2013.

[13] R. Fung, V. Shneerson, D. K. Saldin, and A. Ourmazd, "Structure from fleeting illumination of faint spinning objects in flight," *Nature Physics*, vol. 5, pp. 64–67, 2008.

[14] A. Singer, "From graph to manifold laplacian: The convergence rate," *Appl. Comput. Harmon. Anal.*, vol. 21, pp. 128–134, 2006.

[15] M. Hein, J. Audibert, and U. von Luxburg, "From graphs to manifoldsweak and strong pointwise consistency of graph laplacians," *in: P. Auer, R. Meir (Eds.), Proc. 18th Conf. Learning Theory (COLT), Lecture Notes Comput. Sci.*, pp. 470–485, 2005.

[16] V. Bingelyte, J. Leach, J. Courtial, and M. J. Padgett, "Optically controlled three-dimensional rotation of microscopic objects," *Appl. Phys. Lett.*, vol. 82, p. 829, 2003.

[17] M. K. Kreysing, T. Kieβling, A. Fritsch, D. Christian, J. R. Guck, and J. A. Käs, "The optical cell rotator," *Opt. Express*, vol. 16, no. 21, p. 16984, 2008.

[18] S. K. Mohanty and P. K. Gupta, "Optical micromanipulation methods for controlled rotation, transportation, and microinjection of biological objects," *Methods in Cell Biology*, vol. 82, pp. 563–599, 2007.

[19] C.-H. Lu, N. C. Pégard, and J. W. Fleischer, "Flow-based structured illumination," *Appl. Phys. Lett.*, vol. 102, p. 16115, 2013.

[20] C.-C. Chen, C.-H. Lu, D. Chien, J. Miao, and T.-K. Lee, "Three-dimensional image reconstruction of radiation-sensitive samples with x-ray diffraction microscopy," *Phys. Rev. B*, vol. 84, p. 024112, 2011.

[21] H. Jiang and *et al*, "Quantitative 3d imaging of whole, unstained cells by using x-ray diffraction microscopy," *Proc. Natl. Acad. Sci. USA*, vol. 170, no. 25, pp. 11234–11239, 2010.

[22] A. C. Kak and M. Slaney, *Principles of Computerized Tomographic Imaging*. Society of Industrial and Applied Mathematics, 2001.

[23] C. Wachinger, M. Yigitsoy, E.-J. Rijkhorst, and N. Navab, "Manifold learning for image-based breathing gating in ultrasound and mri," *Medical Image Analysis*, vol. 16, no. 4, pp. 806–818, 2012.

[24] D. S. Biggs, "3d deconvolution microscopy," *Curr. Protoc. Cytom.*, vol. 12, pp. 1–20, 2010.